11th Canadian Masonry Symposium, Toronto, Ontario, May 31- June 3, 2009

BEHAVIOUR OF PARTIALLY GROUTED REINFORCED MASONRY SHEAR WALLS-NUMERICAL STUDY

Majid Maleki[1], A. A. El-Damatty[2], R. G. Drysdale[3], and A. A. Hamid[4]

[1] Ph.D., Centre for Effective Design of Structures, Department of Civil Engineering, McMaster University, Hamilton ON, L8S 4L7, Canada, malekim@mcmaster.ca

[2] Professor, Department of Civil and Environmental Engineering, The University of Western Ontario, London, ON, N6A 5B8, Canada, damatty@uwo.ca

[3] Professor Emeritus, Centre for Effective Design of Structures, Department of Civil Engineering, McMaster University, drysdale@mcmaster.ca

[4] Professor, Department of Civil and Architecture Engineering, Drexel University, Philadelphia, PA, 19104, USA, hamidaa@drexel.edu

ABSTRACT

In this article, a computationally efficient numerical (finite element) technique is presented to simulate the in-plane behaviour of partially grouted reinforced masonry structures with the main focus on single-storey masonry shear walls. An orthotropic smeared crack model is employed with the masonry and reinforcing steel bars represented using adjoining overlaid elements. The interface of mortar joint and masonry unit is modelled using a plasticity model. The proposed model also includes the effect of buckling of vertical reinforcement in the compression zone. The capability of the model in predicting response of partially grouted-reinforced masonry shear walls under in-plane loading is evaluated by direct comparison to experimental results. In general, acceptable accuracy was observed in numerically predicted lateral load carrying capacities and load-displacement curves in both pre- and post-peak regimes.

KEYWORDS: Finite Element, Numerical, Partially Grouted, Reinforced, Shear Wall, Masonry.

INTRODUCTION

Previous studies on fully grouted masonry shear walls under in-plane loading [1,2] have shown that using a smeared crack model with no distinction between masonry units and mortar joints can produce reliable numerical results. This is mainly because grouting diminishes the anisotropy caused by mortar joints. However, in unreinforced or partially grouted reinforced masonry shear walls, one of the dominant failure modes is debonding and slippage at unit-mortar interfaces. This necessitates considering mortar joints as a secondary material phase. In this paper, the behaviour of partially grouted reinforced masonry is modelled using a smeared crack model combined with quadrilateral interface elements representing mortar joints. The model also includes the effect of inelastic buckling of vertical reinforcement in the compression zone. To evaluate the performance of the model, numerical predictions are compared to experimental results.

MODEL FOR MASONRY

In the smeared crack approach, masonry units are represented by similar constitutive relations along the axes of orthotropy that are modified following cracking. These axes coincide with the principal directions of total strain and are continuously updated during analysis. Once the principal tensile stress exceeds the uniaxial tensile strength of masonry in one direction, cracking initiates in the normal direction and the constitutive relations along the existing principal axes are updated [4,5].

Due to the Poisson's effect and microcrack confinement, biaxial stresses alter the strength and constitutive characteristics of masonry compared to those for uniaxial loading. In order to include this behaviour, the masonry strength in each principal direction is modified using the following equations (see Figure 1-a):

$$f_p = \lambda f'_m \qquad \text{and} \qquad \varepsilon_p = \lambda \varepsilon_\circ \tag{1}$$

where f'_m is the uniaxial compressive strength of masonry and ε_o is the strain at f'_m. The parameter f_p is the equivalent compressive strength of biaxially loaded masonry and ε_p is the corresponding strain at f_p. The modification factor, λ, is defined based on the ratio of principal stresses or principal strains at each point. According to the model originally proposed by Kupfer et al. [6], for a *compression-compression* biaxial state of stress, λ acts as an amplification factor increasing the uniaxial compressive strength of masonry based on the following equation

$$\lambda = \frac{1 + A_0 \sigma_1 / \sigma_2}{\left(1 + \sigma_1 / \sigma_2\right)^2} \qquad 0 \le \sigma_1 / \sigma_2 \le 1 \tag{2}$$

where σ_1 and σ_2 are the principal stresses. The parameter A_o is used to adjust the model for different material properties and a value of 3.65 was suggested [6] for concrete. Under a *tension-compression* state of stress, the compressive strength of masonry decreases. In this case, λ defines a reduction factor based on the following set of equations [2]:

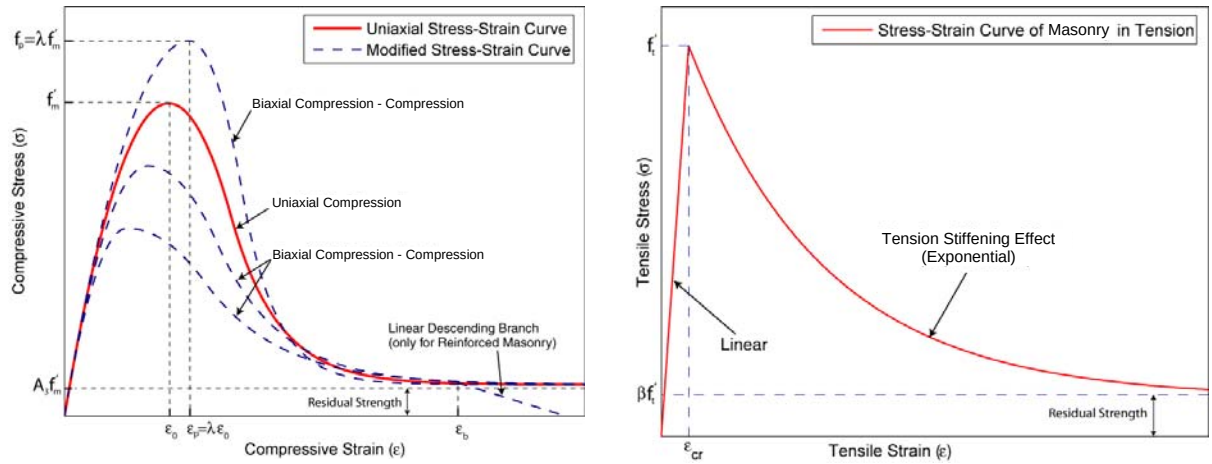

(a) Compression zone (modified under biaxial state of stress)

(b) Tension zone

Figure 1: Stress-strain relationships for masonry

$$\lambda = \begin{cases} 1.0 & \varepsilon_{tens.} / \varepsilon_{comp.} \le 0.56 \\ \left[0.85 - 0.27\left(\varepsilon_{tens.} / \varepsilon_{comp.}\right)\right]^{-1} & 0.56 < \varepsilon_{tens.} / \varepsilon_{comp.} \le 20.0 \\ 0.16 & \varepsilon_{tens.} / \varepsilon_{comp.} > 20.0 \end{cases} \quad (3)$$

where $\varepsilon_{tens.}$ and $\varepsilon_{comp.}$ are the principal tensile and compressive strains, respectively. In the *tension-tension* biaxial combination of stresses, the tensile strength remains equal to the uniaxial properties in both directions of principal strain.

The uniaxial stress-strain relation of masonry, shown in Figure 1-a, is expressed by the following equations [2]:

$$\sigma(\varepsilon) = \begin{cases} f'_m\left[A_1\left(\varepsilon / \varepsilon_\circ\right) - \left(A_1 - 1\right)\left(\varepsilon / \varepsilon_\circ\right)^2 / \lambda\right] & \varepsilon < \varepsilon_p \quad (4) \\ f_p\left[1 - \left(\left(\varepsilon - \varepsilon_p\right) / \left(A_2\varepsilon_\circ - \varepsilon_p\right)\right)^2\right] & \varepsilon_p < \varepsilon \le \varepsilon_e \quad (5) \\ f_e\left[A_3\left(f_m / f_e\right) + \left(1 - A_3\left(f_m / f_e\right)\right)\exp\left(-\gamma\left(\varepsilon - \varepsilon_e\right) / \varepsilon_e\right)\right] & \varepsilon > \varepsilon_e \quad (6) \end{cases}$$

The parameters A_1, A_2, A_3, and A_4 control the shape of the curves and can be adjusted based on masonry's behaviour under uniaxial compression. The parameters ε_e, f_e and γ control the transition from the curve defined by Equation 5 and the one defined by Equation 6 where ε_e is the point of tangency calculated based on the following equation:

$$\varepsilon_e = \varepsilon_\circ\left(1 + \lambda A_4\left(A_2 - 1\right)\right) \quad \text{and} \quad \gamma = 2\lambda\frac{f_m}{f_e} \times \frac{\varepsilon_e}{1 - A_3\left(f_m / f_e\right)} \times \frac{\left(\varepsilon_e - \varepsilon_p\right)}{\left(A_2\varepsilon_\circ - \varepsilon_p\right)^2} \quad (7)$$

It is documented that the failure of a masonry shear wall is mainly initiated by crushing of the compressed toe followed by degradation of the wall's load resistance [7]. The onset of crushing exposes the embedded vertical reinforcing steel bars which then may be subjected to large out-of-plane deformation due to inelastic buckling resulting in rapid degradation of strength at the toe of the wall. For a partially grouted reinforced masonry shear wall, this effect can be quite critical since the large spacing between columns of grouted cells means that crushing and bar buckling in one cell causes a significant decrease in wall strength; the adjacent ungrouted cells cannot compensate effectively for the loss of loadbearing area. This can play a key role in defining the softening response of this type of masonry shear wall after reaching the peak load. Thus, for an accurate simulation of post-peak response of a partially grouted reinforced masonry shear wall, it is necessary to include both the masonry crushing and the effect of buckling of compressive steel reinforcement in the material model of reinforced masonry.

To investigate the behaviour of the compression toe of a partially grouted reinforced masonry shear wall after buckling of embedded vertical reinforcement, a series of uniaxial compressive tests [4] were carried out on reinforced and unreinforced masonry prisms filled with grout. The prisms were three-blocks high and a half-block long simulating the exterior column of grouted

cells in the extreme compression zone of a partially grouted reinforced masonry shear wall as shown in Figure 2. The comparison between the stress-strain relations of the reinforced and unreinforced grouted specimens, as presented in Figure 3, indicates almost linear strength degradation associated with buckling of vertical reinforcement. Accordingly, to reflect this behaviour in the material model used for reinforced masonry, a linear descending branch is added to the end of the stress-strain relation of both masonry and steel within a specified strain range. This behaviour, illustrated in Figure 1-a (also see Figure 4), is defined by:

$$\sigma(\varepsilon) = \sigma_{bm} - A_5(\varepsilon - \varepsilon_b) \le 0 \qquad \varepsilon > \varepsilon_b \tag{8}$$

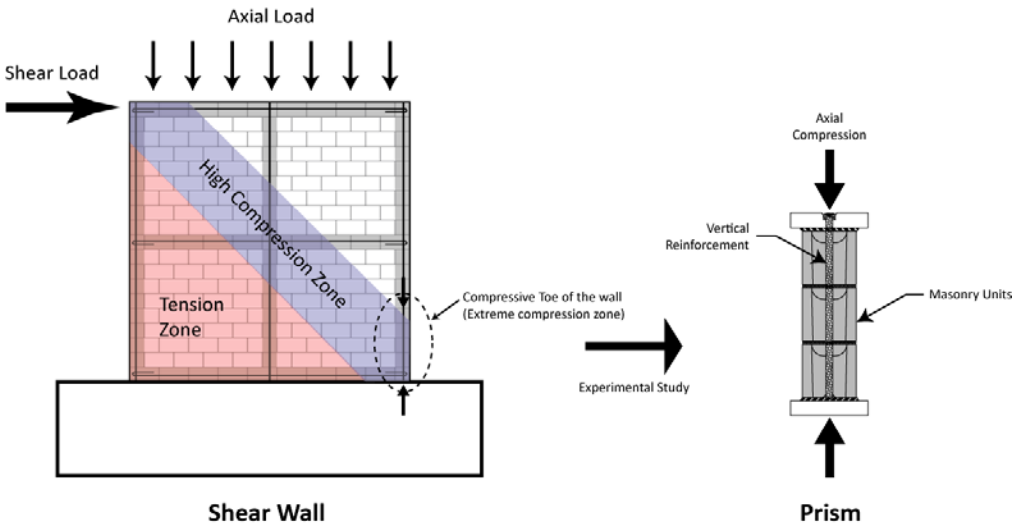

Figure 2: Simulation of compressive toe in the experimental study

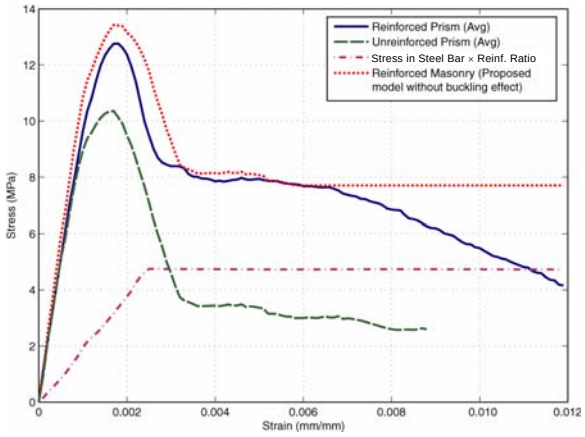

Figure 3: Average stress-strain curves obtained from prism tests

In this equation, ε_b defines the strain at which buckling starts and σ_{bm} is the corresponding stress value determined by Equation 6. The parameter A_5 defines the strength degradation rate due to buckling of a compressive steel bar. According to this model, once strain in masonry reaches the bar buckling limit specified by ε_b, the compressive strength of masonry reduces to zero in a

strain interval approximately equal to:

$$\Delta\varepsilon_b = A_3 f_m / A_5 \tag{9}$$

In this equation, the small exponential terms of Equation 6 are neglected. Similar linear degradation, described in the following section, is assumed for axial resistance of the vertical steel bar at the compressed toe.

The stress-strain relation of masonry in tension is assumed to be independent of lateral compressive stress and is defined by a linear behaviour prior to cracking followed by an exponentially descending branch (Figure 1-b). This relation is defined by:

$$\sigma(\varepsilon) = \begin{cases} E_t \varepsilon & 0 < \varepsilon \le \varepsilon_{cr} \\ f_t' \left[\beta + (1-\beta) \exp\left(-\alpha \left(\varepsilon - \varepsilon_{cr}\right) / \varepsilon_{cr}\right)\right] & \varepsilon > \varepsilon_{cr} \end{cases} \tag{10}$$

The parameter β controls the lower limit of the exponential branch and α incorporates the effect of tension stiffening [2] where ε_{cr} is the strain at which masonry cracks. The constitutive model used for masonry prior to tensile cracking is defined by [2]:

$$\mathbf{D_m} = \frac{1}{1-\nu^2} \begin{bmatrix} E_1 & \nu\left(E_1 E_2\right)^{1/2} & 0 \\ \nu\left(E_1 E_2\right)^{1/2} & E_2 & 0 \\ 0 & 0 & (1-\nu^2)G \end{bmatrix} \tag{11}$$

where E_1 and E_2 can be either the secant or the tangent moduli of elasticity in the directions of the principal axes of total strains. The parameter ν is Poisson's ratio and G is the shear modulus. After tensile cracking, due to loss of correlation between deformations in the principal directions the diagonal terms in the constitutive matrix vanish.

MODEL FOR STEEL

As shown in Figure 4, the stress-strain relationship for steel before and after yielding is represented by an idealized bilinear strain hardening behaviour that is assumed to be identical in tension and compression. Similar to the masonry model, the effect of buckling of the reinforcing steel bar is simply represented by a linear descending branch attached to the stress-strain curve of steel in compression. This behaviour is consistent with the experimental evidence provided by the uniaxial compression tests on reinforced masonry prisms [4]. Strength degradation due to buckling of the reinforcement starts at ε_b which is the same buckling strain as defined in the masonry model. The degradation rate of the reinforcing steel bar is defined by:

$$R_b = \frac{\sigma_{bs} - \sigma_r}{\Delta_b} \tag{12}$$

where σ_{bs} is the stress corresponding to ε_b at which point buckling initiates and σ_r is the residual stress in the reinforcing bar after buckling. Parameter Δ_b was previously defined by Equation 9.

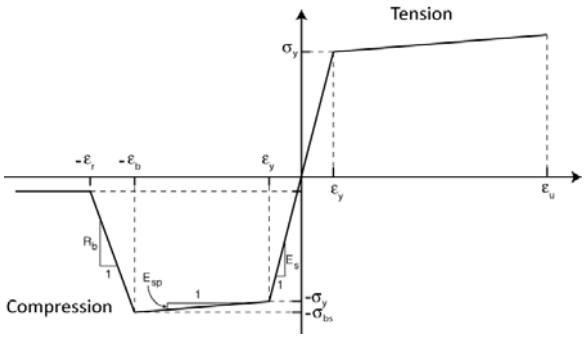

Figure 4: Uniaxial stress-strain relation for steel

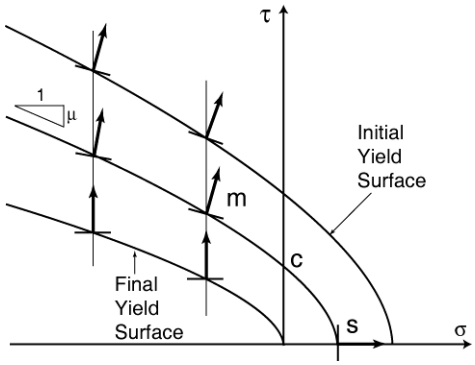

Figure 5: Yield surface and evolution of plastic potential for unit-mortar interface [8]

MODEL FOR UNIT-MORTAR INTERFACE

To accommodate the effects of the inherent anisotropy in masonry due to the presence of mortar joints, a constitutive model is incorporated in a plasticity framework. The model, adopted from Lotfi [8], includes initiation and propagation of fracture along the unit-mortar interface under combined normal and shear stresses and incorporates joint dilatancy. As the elastic limit, the yield criterion is described by a three-parameter hyperbolic surface that provides a smooth transition between the Mohr-Coulomb and tension-cut-off yield criteria (Figure 5). The dilatant behaviour, originating from the roughness of the fractured surfaces, is also included using a nonassociated flow rule. The evolution of the plastic potential surface is illustrated in Figure 5. In this model, the softening behaviour of the unit-mortar interface is governed by preserving the Mode-I and Mode-II fracture energies per unit volume during strength degradation [8].

FINITE ELEMENT PROGRAM

The nonlinear constitutive relations, described in the previous sections, are implemented in a displacement-driven finite element program developed as part of this study. Plane stress, isoparametric, eight-noded elements are used for the masonry blocks and plane stress, six-noded contact elements are used for the unit-mortar interface. The elastic behaviour of the joints is considered in the stiffness matrix of interface elements. As illustrated in Figure 6, the contributions of horizontal and vertical steel reinforcement are included using an adjoining overlaid element. Despite the assumption of perfect bond, the interaction between grout and steel bar is implicitly considered in the tension stiffening model of the masonry. Since the conventional or modified Newton-Raphson iteration scheme fails to converge in the vicinity of peak loads, the arc-length incremental algorithm [9] is employed as the solution strategy and a convergence criterion based on the norm of nodal displacement vectors is used with a convergence threshold of 0.001 [2,8].

EVALUATION OF THE PROPOSED MODEL

The performance of the model was evaluated by simulating the response of five partially grouted reinforced masonry shear wall tests under combined axial and lateral loading [4]. Details of the testing program and their results are reported in a companion paper [3] in this symposium. The finite element model for Wall 1 of the test walls, as a typical model used to simulate the behaviour of partially grouted reinforced masonry shear walls with aspect ratio of one, is

illustrated in Figure 7. Shear walls are modelled using eight-node elements for masonry and six-node interface elements for mortar head and bed joints. The properties of the top row of elements for each wall together with the "mortar head joints" between these elements are modified to represent the effect of the relatively rigid loading beam utilized in the experiments. These loading beam elements are assumed to behave in a linear elastic manner with a relatively high dummy value for the elastic moduli (i.e., 100 times higher than masonry elements). The top nodes also are programmed to have equal displacement in the x-direction. The nodes at the bottom of the finite element model are restrained against displacements in both the x- and y-directions assuming perfect contact between the shear wall and the concrete base.

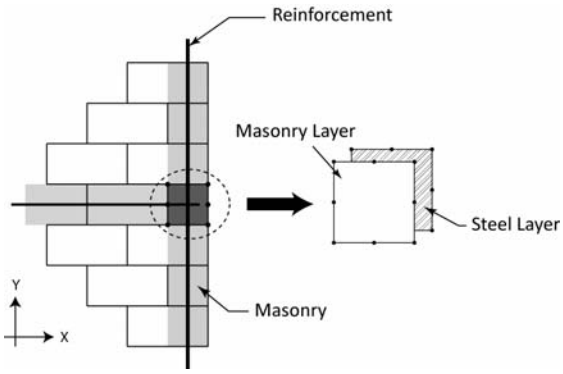

Figure 6: Layered element employed for reinforced masonry model

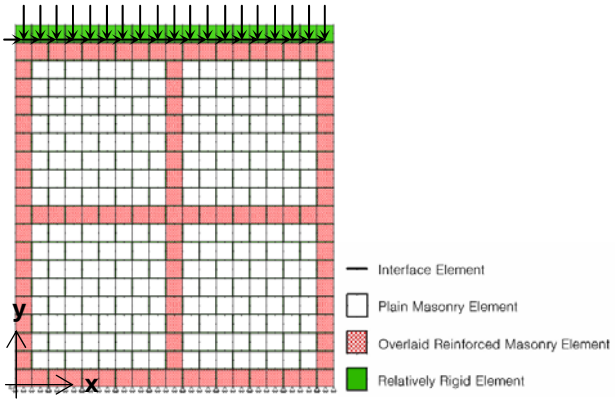

Figure 7: Finite element model for Wall 1

MATERIAL PROPERTIES

The material properties used for the masonry elements are presented in Table 1. The uniaxial compressive strength, f'_m, and the corresponding masonry strain, ε_m, are chosen based on the results of the uniaxial compressive tests on four-block-high masonry prisms constructed at the same time as shear walls. The tensile cracking strength of ungrouted masonry units, f_{cr}, is set to f_{cr}=0.1 f'_m recommended for masonry materials [7]. The constitutive parameters concerning the stress-strain relationship and biaxial strength envelope of masonry (A_o, A_1, A_2, A_3, A_4, and α and β) are adopted from other similar studies [1,2,5].The parameters related to the effect of bucking of reinforcing steel bars in the compression zone are based on the results of the uniaxial compression tests of the reinforced masonry prisms shown in Figure 3. A value of $\varepsilon_b = 2.5\varepsilon_y$ is used as the initial buckling strain and the degradation rate is set to A_5 = 640 MPa according to the auxiliary test results. The buckling is assumed to be completed in a strain interval of $\Delta_b = 2.5\varepsilon_b$.

Owing to the similarity of the constituent material and construction conditions, the initial tensile bond strength, s_o, initial cohesive strength, r_o, and initial shear friction coefficients of the unit-mortar interface elements, presented in Table 2, are based on experimental and numerical studies of the behaviour of partially grouted reinforced concrete masonry panels under in-plane diagonal loading [4,5]. The remainder of the parameters, defining the shape of the yield and plastic potential surfaces along with the softening rules, are adopted from Lotfi [8]. Similar to other studies [8], the elastic properties of the mortar are adjusted to reproduce the initial stiffness of Wall 1 and remained the same for the other test walls. The geometric and mechanical properties

for steel bars obtained from the tensile tests are presented in Table 3.

Table 1: Material properties for masonry

Masonry Property	Hollow	Grouted
f'_m (N/mm^2)	21.1	12.0
ε_m (mm/mm)	0.0013	0.0013
f_{cr} (N/mm^2)	2.65	1.2
E_m (N/mm^2)	20000	20000
v	0.16	0.16
α	0.5	0.2
β	0.1	0.1
A_o	3.65	3.65
A_1	2.0	2.0
A_2	2.0	2.0
A_3	0.1	0.1
A_4	0.6	0.6

Table 2: Material properties for mortar joints

Joint Properties	Bed Joint	Head Joint
D_{nn} (N/mm^2/mm)	400	400
D_{tt} (N/mm^2/mm)	200	200
s_0 (N/mm^2)	0.8	0.6
r_0 (N/mm^2)	0.8	0.6
r_r (N/mm^2)	0.035	0.035
μ_0	0.95	0.75
μ_r	0.60	0.45
α, β (mm/N)	11.4	11.4
η	0.1	0.2
$G^f_{\min} \times 10^{-3}$ (N.mm/mm^2)	0.8	0.45
$G^f_I \times 10^{-3}$ (N.mm/mm^2)	4.0	2.25
$G^f_{II} \times 10^{-3}$ (N.mm/mm^2)	40	22.5

Table 3: Geometric and mechanical properties of steel reinforcement

Bar Type	Area (mm^2)	E_s (GPa)	f_y (MPa)	ε_y (mm/mm)
No. 10 (CA Size)	100	201.6	491.7	0.0024
No. 3 (USA Size)	71	201.0	485.0	0.0024
No. 4 (USA Size)	126	201.8	564.7	0.0028
D3 (USA Size)	19.4	183.6	743.7	0.0041
D4 (USA Size)	25.8	198.2	690.7	0.0035

NUMERICAL VERSUS EXPERIMENTAL RESULTS

The ultimate load carrying capacity and corresponding lateral top displacement of the test walls predicted by the numerical model are presented in Table 4 along with the values measured during the tests. The ultimate strengths of the walls indicate that wider bar spacing corresponds with slightly lower wall strength. It can also be seen that less than 10% difference exists between the numerical estimations and the measured values.

The numerical and experimental load-displacement curves for Wall 1 are shown in Figure 8 as an example. The envelopes of the experimental hysteresis loops in both the push and pull directions are used as the experimental load-displacement curves. As shown, satisfactory agreement exists between the predicted load-displacement responses and the actual behaviours during the test. Similar agreement is also found between numerical and experimental load-displacement curve of the other shear wall tests.

In the finite element simulation of the Wall 1 test, buckling of the compressive steel bar

($\varepsilon_{comp.} > \varepsilon_b$), located in the bottom right corner masonry element, started shortly after reaching the maximum load resistance of the wall (after approximately 5% load degradation). At approximately 4 mm top displacement, crushing ($\varepsilon_{comp.} > \varepsilon_p$) covered more than 50% of the integration points of the bottom right corner masonry elements. This agrees fairly well with the average top displacement at which the bottom corner blocks at both toes of the actual test wall ARE crushed [4]. Similar agreement IS also observed for the other test walls.

Table 4: Numerical and experimental results for shear wall tests

Shear Wall (Bar Spacing) [Aspect ratio]	Property	Numerical	Experimental		Num. / Exp.	
			Push	Pull	Push	Pull
Wall 1 (855 mm) [1.0]	Ultimate Load	94.71 kN	91.2 kN	96.9 kN	1.04	0.98
	Top Disp.	2.42 mm	2.88 mm	2.88 mm	0.84	0.84
Wall 2 (570 mm) [1.0]	Ultimate Load	96.73 kN	103.7 kN	93.2 kN	0.93	1.04
	Top Disp.	2.40 mm	4.50 mm	3.24 mm	0.53	0.74
Wall 3 (1710 mm) [1.0]	Ultimate Load	91.53 kN	96.7 kN	84.4 kN	0.95	1.08
	Top Disp.	3.49 mm	3.60 mm	2.34 mm	0.97	1.49
Wall 4 (855 mm) [0.5]	Ultimate Load	122.3 kN	114.2 kN	122.9 kN	1.07	1.00
	Top Disp.	0.52 mm	0.80 mm	0.81 mm	0.65	0.64
Wall 5 (855 mm) [1.5]	Yield Load	70.0 kN	70.5 kN	73.2 kN	0.99	0.96
	Top Disp.	4.76 mm	6.03 mm	6.87 mm	0.79	0.69
	Ultimate Load	72.8 kN	79.1 kN	84.3 kN	0.92	0.86
	Disp.	5.58 mm	8.91 mm	10.8 mm	0.63	0.52

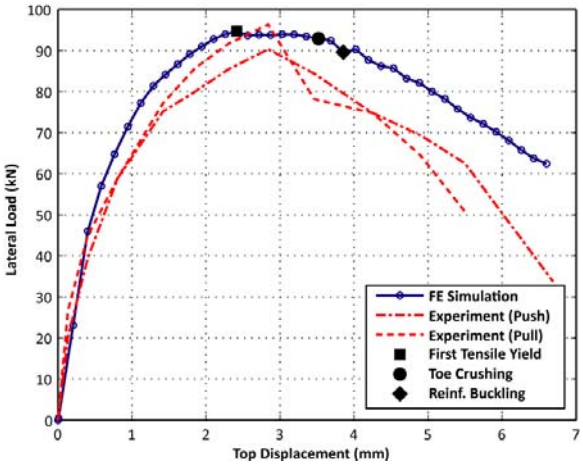

Figure 8: Experimental and finite element load-displacement responses for Wall 1 (aspect ratios $h/\ell = 1.0$)

The finite element analyses of Walls 1, 2, 3 and 4 predicted similar failure modes for each wall. Horizontal tensile cracking started to propagate at the bottom courses of the walls at about 50% of the ultimate load. The failure modes of the walls were characterized by crushing of the

compression toes and buckling of compressive reinforcing steel bars followed by widening of joint cracks. No major yielding or buckling of steel bars was detected in the finite element model of the wall; this is consistent with experimental observations and the shear dominated failure mode for this wall. As indicated in Table 4, only Wall 5 (aspect ratio 1.5) experienced tensile yielding before reaching the peak load. This also is in close agreement with the experimental results.

CONCLUSIONS

Building on previous models developed in reinforced and unreinforced masonry studies, a computationally efficient numerical technique was introduced for analysis of the behaviour of partially grouted reinforced masonry shear walls. The performance of the numerical model was evaluated by simulation of shear wall tests [3] carried out as part of the same study. In general, very good agreement was observed between the experimental results and the finite element predictions in terms of the pre- and post-peak response, ultimate load carrying capacity, and failure sequence.

REFERENCES

1. Maleki, M., El-Damatty, A. A., Hamid A. A., and Drysdale R. G. (2008), "Finite Element Analysis of Reinforced Masonry Sear Walls Using Smeared Crack Model", Tenth Canadian Masonry Symposium, Banff, Alberta
2. Ewing, R. D., El-Mustapha, A. M., Kariotis, J. C. (1987), "FEM/I – A Finite Element Computer Program for the non-linear Static Analysis of Reinforced Masonry Building Components", U.S. – Japan Coordinate program for masonry Building research, Report No. 2.2-1
3. Maleki, M., El-Damatty, A. A., Drysdale, R. G. and Hamid, A. A. (2009), "Behaviour of Partially Grouted Reinforced Masonry Shear Walls; Experimental Study", 11th Canadian Masonry Symposium, Toronto, Ontario
4. Maleki, M. (2008), "Behaviour of Partially Grouted Reinforced Masonry Shear Walls under Cyclic Reversed Loading", Ph.D. Thesis, Department of Civil Engineering, McMaster University, Hamilton, Ontario
5. Maleki, M., Hamid, A. A., El-Damatty, A. A. and R. G. Drysdale (2007), "Behaviour of Partially Grouted Reinforced Concrete Masonry Panels under In-Plane Diagonal Loading", Tenth North American Masonry Conference, St. Louis, Missouri
6. Kupfer H. B., Hilsdorf H. K., Rusch H. (1969), "Behavior of Concrete under Biaxial Stresses", ACI Journal, Vol. 66, No. 8, pp. 656-666
7. Drysdale, R., and Hamid, A. A., (2005), "Masonry Structures: Behaviour and Design", Canadian Masonry Design Centre, Mississauga, ON
8. Lotfi, H. R., and Shing, P. B. (1994), "Interface Model Applied to Fracture of Masonry Structures", Journal of Structural Engineering, vol. 120, no. 1, pp. 63-80
9. Crisfield, M. (1997), "Nonlinear Finite Element Analysis of Solids and Structures", John Wilely & Sons, Inc., New York, New York